Supporting Information

Inclusion of Gold Ion in Tiara-Like Nickel Hexanuclear Nanocluster

Kana Takemae,[a,†] Shiho Tomihari,[a,†] Takumi Naito,[b] Makito Takagi,[b] Tomomi Shimazaki,[b] Tokuhisa Kawawaki,*[a,c] Masanori Tachikawa*[b] and Yuichi Negishi*[c,d]

[a]Department of Applied Chemistry, Faculty of Science, Tokyo University of Science, 1-3 Kagurazaka, Shinjuku−ku, Tokyo 162−8601, Japan

[b]Quantum Chemistry Division, Yokohama City University, 22-2 Seto, Kanazawa-ku, Yokohama, 236-0027, Japan

[c]Research Institute for Science and Technology, Tokyo University of Science, 1-3 Kagurazaka, Shinjuku-ku, Tokyo 162–8601, Japan

[d]Institute of Multidisciplinary Research for Advanced Materials, Tohoku University, 2-1-1 Katahira, Aoba-ku, Sendai 980-8577, Japan

*Corresponding Author E-mail: kawawaki@rs.tus.ac.jp (T. K.), tachi@yokohama-cu.ac.jp (M. T.) yuichi.negishi.a8@tohoku.ac.jp (Y. N.)

†These authors contributed equally to this work.

1 Chemicals

All chemicals were commercially obtained and used without further purification. nickel(II) nitrate hexahydrate [$Ni(NO_3)_2{\cdot}6H_2O$], triethylamine [$(CH_3CH_2)_3N$], boron nitride [BN], silver(I) chloride [AgCl], chromium(VI) oxide [CrO_3], manganese(II) chloride tetrahydrate [$MnCl_2{\cdot}4H_2O$], iron(II) chloride tetrahydrate [$FeCl_2{\cdot}4H_2O$], cobalt(II) nitrate hexahydrate [$Co(NO_3)_2{\cdot}6H_2O$], copper(II) chloride [$CuCl_2$], zinc(II) chloride [$ZnCl_2$], ruthenium(III) chloride n-hydrate [$RuCl_3{\cdot}nH_2O$], rhodium(III) chloride trihydrate [$RhCl_3{\cdot}3H_2O$], cadmium(II) chloride [$CdCl_2$], indium(III) chloride tetrahydrate [$InCl_2{\cdot}4H_2O$], 5% Nafion™ Dispersion Solution DE521 CS type and palladium(II) acetate [$Pd(CH_3COO)_2$] were obtained from FUJIFILM Wako Pure Chemical Co (Japan). Perchloric acid, acetonitrile (MeCN), methanol (MeOH), hexane, tetrahydrofuran (THF), toluene and dichloromethane (DCM) were obtained from Kanto Chemical Co., Inc (Japan). *trans*-2-[3-(4-*tert*-butylphenyl)-2-methyl-2-propenylidene]malononitrile (DCTB) and (triphenylphosphine)gold(I) chloride [Ph_3PAuCl] were obtained from Tokyo Kasei (Japan). Hydrogen tetrachloroaurate(III) tetrahydrate [$HAuCl_4{\cdot}4H_2O$] and hydrogen hexachloroplatinate(IV) hexahydrate [$H_2PtCl_6{\cdot}6H_2O$] were purchased from Tanaka Kikinzoku. 2-phenylethanethiol was obtained from Sigma–Aldrich (USA). Pure Milli-Q water (>18 MΩ·cm) was generated using a Merck Millipore Direct 3 UV system.

2. Characterization

Ni K-edge X-ray absorption fine structure (XAFS) measurements were performed at beamline BL01B1 of the SPring-8 facility of the Japan Synchrotron Radiation Research Institute (proposal numbers 2022B1823, 2023A1675 and 2023B1825). The incident X-ray beam was monochromatized by a Si(111) double-crystal monochromator. As references, XAFS spectra of Ni foil, and solid NiO were recorded in transmission mode with ionization chambers. The Ni K-edge XAFS spectra of the samples were measured in transmission mode with ionization chambers at room temperature. The X-ray energies for the Ni K-edges were calibrated using Ni foil. The X-ray absorption nearedge structure (XANES) and extended XAFS (EXAFS) spectra were analyzed using xTunes[1] as follows. The χ spectra were

extracted by subtracting the atomic absorption background using cubic spline interpolation and normalized to the edge height. The normalized data were used as the XANES spectra. The k^3-weighted χ spectra in the k range 3.0–14.0 $Å^{-1}$ for the Ni K-edge were Fourier transformed into r space for structural analysis.

The Au $4f_{7/2}$, Ni 2p and S 2p X-ray photoelectron spectroscopy (XPS) spectra were collected by using a JPS-9010MC electron spectrometer (JEOL, Tokyo, Japan) at a base pressure of ~2×10^{-8} Torr. X-rays from the Mg-Kα line (1253.6 eV) were used for excitation. Each nanoclusters (NCs) was deposited on an Ag plate and the spectra were calibrated with the peak energies of Ag $3d_{5/2}$ (368.22 eV).

The ultraviolet-visible absorption spectra of products were acquired in DCM and THF solution at room temperature with a V-630 spectrometer (JASCO, Tokyo, Japan).

Fourier transform infrared (FT-IR) spectra of the product were obtained using the attenuated total reflectance (ATR) method in the region between 400 and 4000 cm^{-1} by a FT/IR-4600-ATR-PRO ONE spectrometer (JASCO, Tokyo, Japan) equipped with a DLATGS detector as the average of 50 scans at 4 cm^{-1} resolution.

The matrix assisted laser desorption/ionization (MALDI) mass spectra were recorded with a JMS-S3000 spiral time-of-flight mass spectrometer (JEOL, Tokyo, Japan) equipped with a semiconductor laser ($\lambda = 349$ nm). DCTB was used as the MALDI matrix. To minimize NCs dissociation induced by laser irradiation, the NC-to-matrix ratio was fixed at 1:1000.

Inductively coupled plasma-mass spectrometry (ICP-MS) was performed with an Agilent 7500c spectrometer (Agilent Technologies, Tokyo, Japan). Bismuth and yttrium was used as the internal standard.

3. DFT Calculation

All calculations were performed with the Gaussian 16 package[2]. The ground-state structures were optimized by density functional theory (DFT) with B3LYP using the Lanl2DZ basis set for metal atoms (Ni, Au) and the 6-31G(d) basis set for the other atoms. Based on the optimized ground-state structure, absorption spectra were calculated using the time-dependent density functional theory (TD-DFT). Here, we considered 400 states to obtain the excited state in the vacuum and the solvent. For calculations considering the solvation effect of THF, the Polarizable Continuum Model (PCM) using the integral equation formalism (IEFPCM) was used.

4. Table

Table S1. Possible assignments for the MALDI-MS spectra in Fig. 2.

Calculated Molecular Weight (*m*/*z*)	Chemical formula
1998	$[Ni_6(SC_8H_9)_{12}]^+$
1666	$[Au_2Ni_3(SC_8H_9)_8]^+$
2195	$[AuNi_6(SC_8H_9)_{12}]^+$
2527	$[AuNi_7(SC_8H_9)_{14}]^+$
2861	$[AuNi_8(SC_8H_9)_{16}]^+$

Table S2. Possible assignments for the MALDI-MS spectra in Fig. S7(A).

Calculated Molecular Weight (*m*/*z*)	Chemical formula
1998	$[Ni_6(SC_8H_9)_{12}]^+$
2061	$[CuNi_6(SC_8H_9)_{12}]^+$
2105	$[AgNi_6(SC_8H_9)_{12}]^+$
2395	$[CuNi_7(SC_8H_9)_{14}]^+$

Table S3. Inclusion energy of $[MNi_6(PET)_{12}]^+$ (*M* = Au, Ag and Cu) in THF using DFT calculations.

Metal ion (*M*)	Au	Ag	Cu
Inclusion energy (kcal/mol)	63.0	31.1	44.8
Mulliken charge on *M* (e)	0.61	1.02	1.10
Natural bond order (NBO) charge on *M* (e)	0.21	0.55	0.57
Averaged bond order of *M*–Ni	0.17	0.07	0.08
Averaged bond order of *M*–S	0.06	0.05	0.04

Table S4. Molecular distances from the optimized structure for $[Ni_6(PET)_{12}]^0$ and $[AuNi_6(PET)_{12}]^+$ in THF using DFT calculations.

Sample	Ni–S (Å)	Ni–Ni (Å)	Center–Ni (Å) Au–Ni (Å)
$Ni_6(PET)_{12}$	2.279 ± 0.0073	3.027± 0.0433	3.027± 0.0644
$AuNi_6(PET)_{12}$	2.277 ± 0.0082	2.939 ± 0.0523	2.937 ± 0.1036

Table S5. Possible assignments for the MALDI-MS spectra in Fig. 5(A).

Calculated Molecular Weight (*m*/*z*)	Chemical formula
2308	$[Pd_6(SC_8H_9)_{12}+Na]^+$
2285	$[Pd_6(SC_8H_9)_{12}]^+$
1967	$[CuPd_5(SC_8H_9)_{10}]^+$
2349	$[CuPd_6(SC_8H_9)_{12}]^+$
2393	$[AgPd_6(SC_8H_9)_{12}]^+$
2774	$[AgPd_7(SC_8H_9)_{14}]^+$

Table S6. Possible assignments for the MALDI-MS spectra in Fig. 5(B).

Calculated Molecular Weight (*m*/*z*)	Chemical formula
2347	$[Pt_5(SC_8H_9)_{10}]^+$
2816	$[Pt_6(SC_8H_9)_{12}]^+$
2880	$[CuPt_6(SC_8H_9)_{12}]^+$
2924	$[AgPt_6(SC_8H_9)_{12}]^+$
3349	$[CuPt_7(SC_8H_9)_{14}]^+$
3394	$[AgPt_7(SC_8H_9)_{14}]^+$
3755	$[Pt_8(SC_8H_9)_{16}]^+$

Table S7. Possible assignments for the MALDI-MS spectra in Fig. S13−15.

Calculated Molecular Weight (*m*/*z*)	Chemical formula
1332	$[Ni_4(SC_8H_9)_8]^+$
1666	$[Au_2Ni_3(SC_8H_9)_8]^+$
2195	$[AuNi_6(SC_8H_9)_{12}]^+$
2527	$[AuNi_7(SC_8H_9)_{14}]^+$
2861	$[AuNi_8(SC_8H_9)_{16}]^+$
1664	$[Ni_5(SC_8H_9)_{10}]^+$
2105	$[AgNi_6(SC_8H_9)_{12}]^+$
1998	$[Ni_6(SC_8H_9)_{12}]^+$
2061	$[CuNi_6(SC_8H_9)_{12}]^+$
2395	$[CuNi_7(SC_8H_9)_{14}]^+$

5. Additional Figures

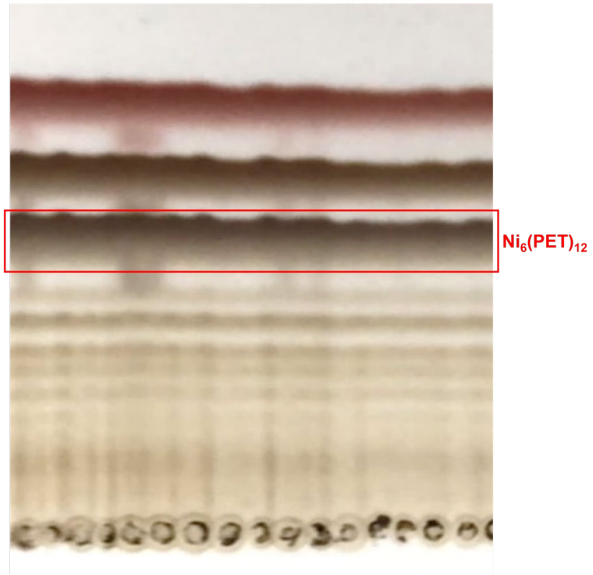

Fig. S1 Photograph of the TLC plate after separation of the synthesized $Ni_n(PET)_{2n}$.

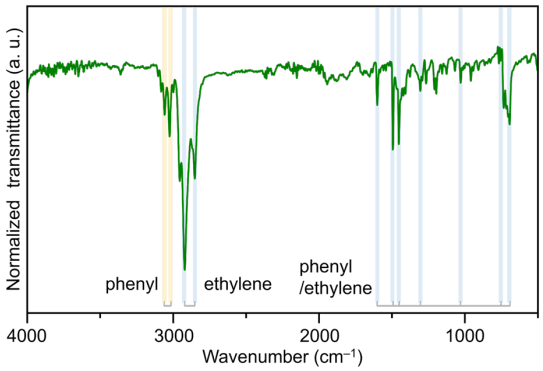

Fig. S2 FT-IR spectra of the synthesized $Ni_6(PET)_{12}$. Absorption around 3000 cm^{-1} and that between 800 and 1500 cm^{-1} indicate that PET are include as a ligand in $Ni_6(PET)_{12}$.[3-6]

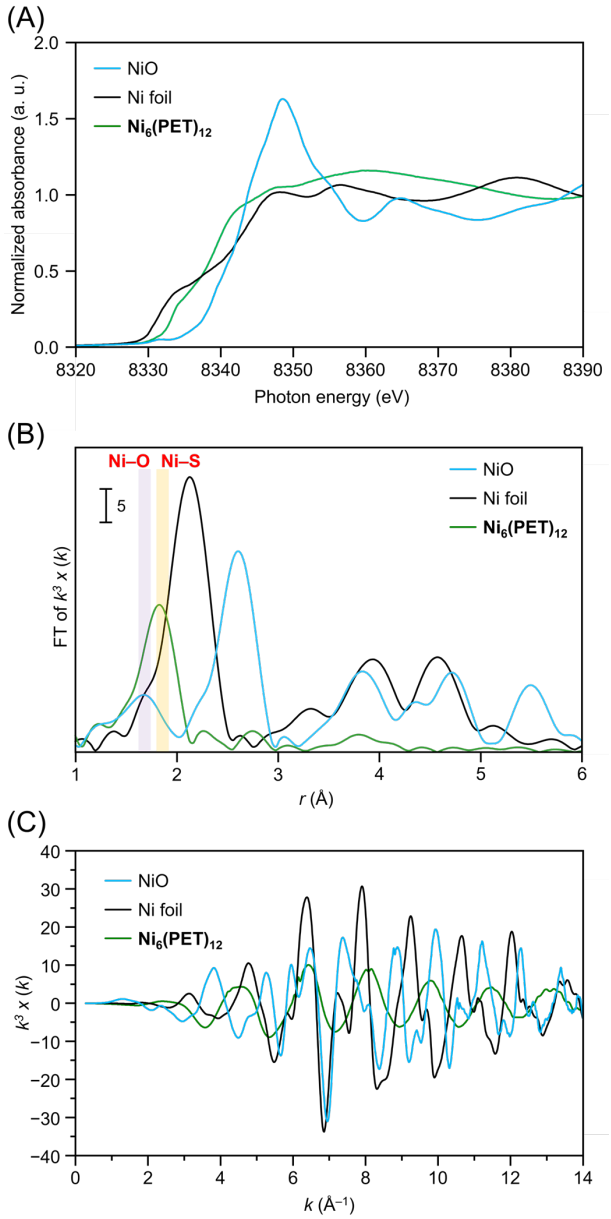

Fig. S3 Results of Ni K-edge (A) XANES, (B) FT-EXAFS and (C) EXAFS spectra for the synthesized $Ni_6(PET)_{12}$ together with Ni foil and NiO. In (B), the peak at ~1.8 Å is assigned to the Ni−S bond. [7]

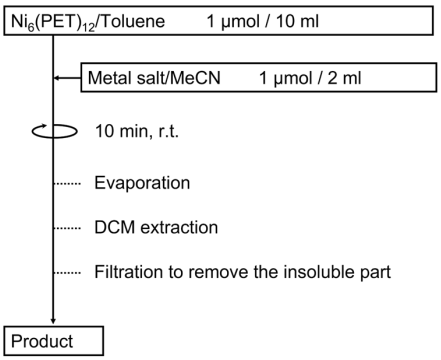

Fig. S4 Protocol used for the screening of the metal ion inclusion into $Ni_6(PET)_{12}$.

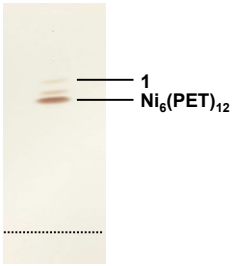

Fig. S5 Photograph of the TLC plate after separation of the synthesized **1**.

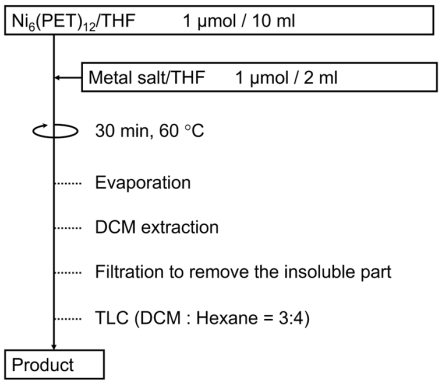

Fig. S6 Protocol used for the metal ion (= Cu, Ag, Au) inclusion into $Ni_6(PET)_{12}$.

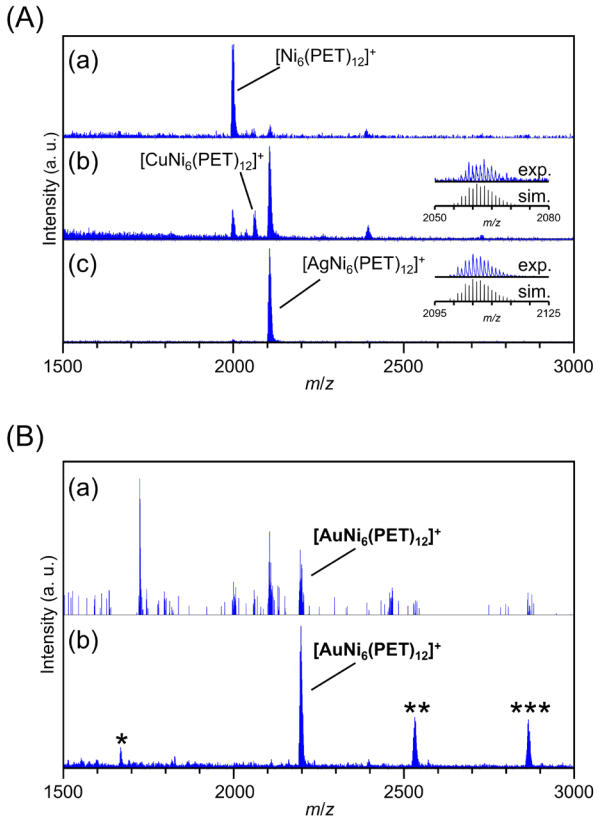

Fig. S7 Positive-ion MALDI-MS spectra of (A) (a) $Ni_6(PET)_{12}$ and those after inclusion of (b) Cu and (c) Ag ion. (B) Positive-ion MALDI-MS spectra after Au ion inclusion into $[Ni_6(PET)_{12}]^0$ when (a) $(Ph_3P)AuCl$ and (b) $HAuCl_4$ were used as a precursor (Au^+ or Au^{3+}). Insets show the comparison of the isotope patterns between experimental spectra (blue) and calculated one (black). In (a) and (b), the relative high intensity at m/z = ~2100 attributed from contamination of $AgNi_6(PET)_{12}$ on the measurement plate for MALDI.

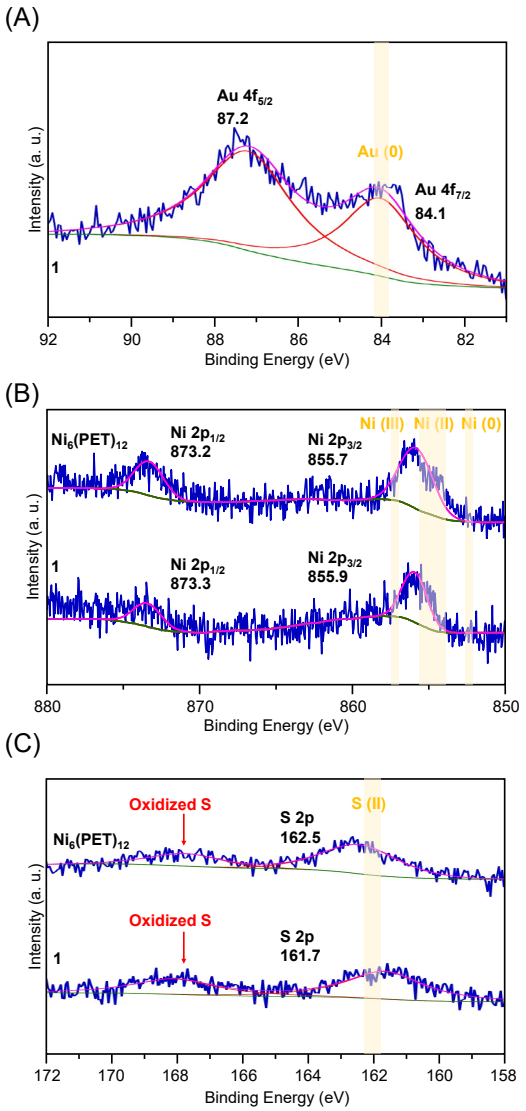

Fig. S8. (A) Au $4f_{7/2}$, (B) Ni 2p and (C) S 2p XPS spectra of $[Ni_6(PET)_{12}]^0$ and **1**. In these figures, the red and pink curves are the fitting results and the green curve is the baselines. Yellow vertical lines indicate the position of Au(0) Ni(0), Ni(II), Ni(III) and S(II), respectively.

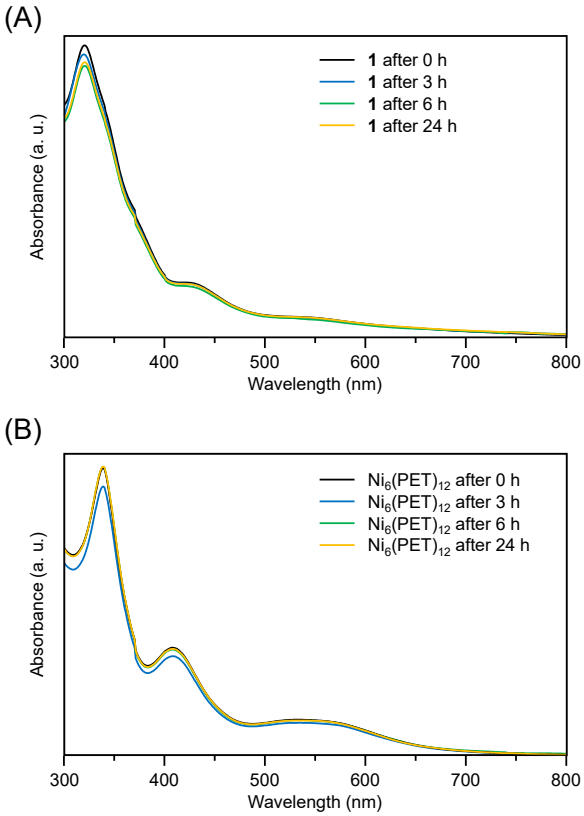

Fig. S9. Time dependence of optical absorbance spectra of (A) **1** and (B) $[Ni_6(PET)_{12}]^0$ at room temperature in THF solution.

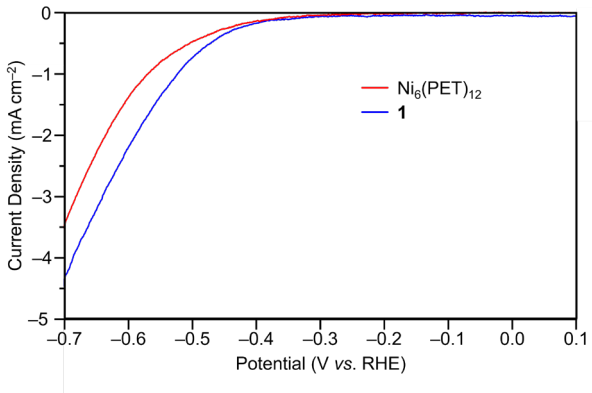

Fig. S10 The results of electrochemical hydrogen evolution reaction (HER) for **1** and $Ni_6(PET)_{12}$. All electrochemical measurements were performed using three electrode system with a glassy carbon disk electrode (GDE; φ = 5 mm) as a working electrode, a silver/silver chloride (Ag/AgCl) electrode as a reference electrode and a Pt coil as a counter electrode. In the setup, first 10 μL of the catalyst slurry which contains 0.018 mg of **1** or 0.017 mg of $Ni_6(PET)_{12}$ with Nafion™, was carefully dropped onto the GDE to load the same amount of Ni. After the catalyst slurry was sufficiently dried, each electrode was set in an electrochemical measurement system containing 0.10 mol L^{-1} $HClO_4$ (pH = 1) as the electrolyte. In the measurements, argon (Ar) gas was bubbled for 30 min and linear sweep voltammetry was performed from 0.5 to −1.0 V *vs*. RHE at a rate of 20 mV s^{-1} under Ar flow.

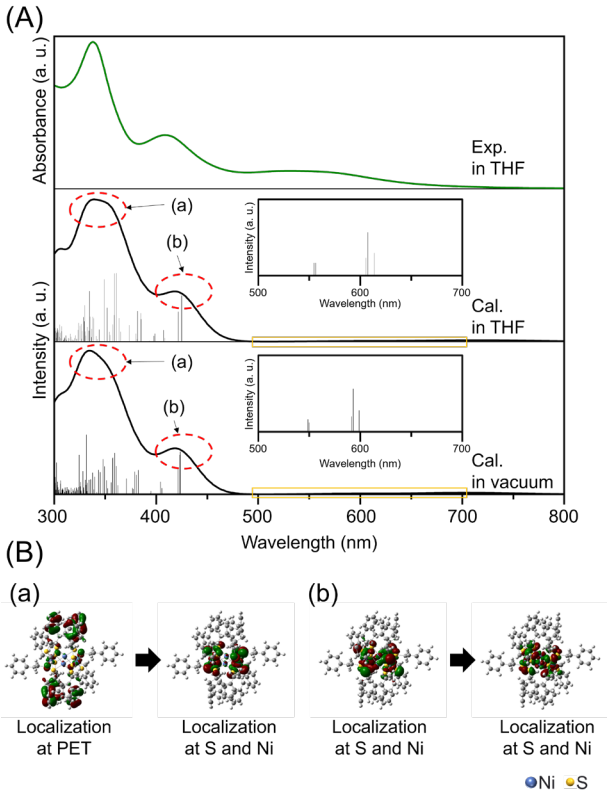

Fig. S11 (A) Experimental (green) and calculated (black) absorption spectra for $[Ni_6(PET)_{12}]^0$ in THF and vacuum. (B) (a)(b) Molecular orbitals of $[Ni_6(PET)_{12}]^0$ for main peaks observed in the optical absorption spectra in THF at (a) and (b) in (A).

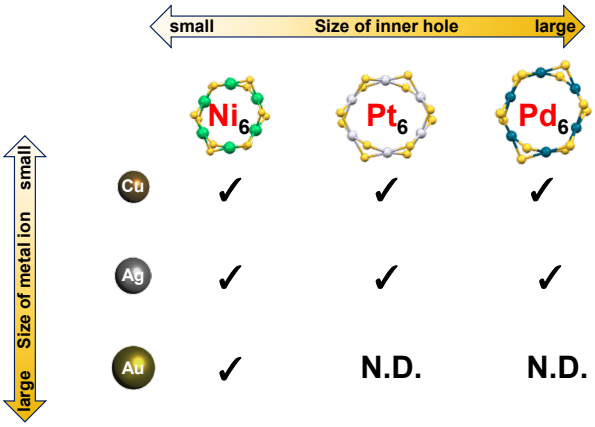

Fig. S12 Relationship between the size of metal ion (Cu, Ag and Au) and the size of inner hole of $[M_6(SR)_{12}]^0$ (M = Ni, Pd, Pt) elucidated by positive-ion MALDI-MS spectroscopy (Fig. 2(A), 5 and S7). The peaks attributed to $[CuNi_6(PET)_{12}]^+$, $[AgNi_6(PET)_{12}]^+$, $[AuNi_6(PET)_{12}]^+$, $[CuPd_6(PET)_{12}]^+$, $[AgPd_6(PET)_{12}]^+$, $[CuPt_6(SR)_{12}]^+$ and $[AgPt_6(SR)_{12}]^+$ were observed in MALDI-MS spectra.

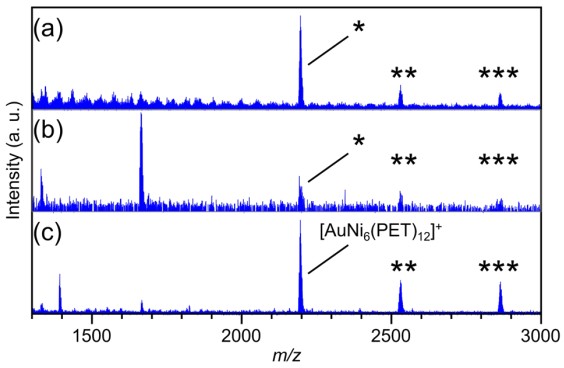

Fig. S13 Positive-ion MALDI-MS spectra of (a) $Ni_4(PET)_8$, (b) $Ni_5(PET)_{10}$ and (c) $Ni_6(PET)_{12}$ after the addition of Au ions. The peaks with "*", "**" and "***" were assigned as $[AuNi_6(PET)_{12}]^+$, $[AuNi_7(PET)_{14}]^+$ and $[AuNi_8(PET)_{16}]^+$, respectively. These spectra demonstrate that no Au ion can be included into $Ni_4(PET)_8$ and $Ni_5(PET)_{10}$.

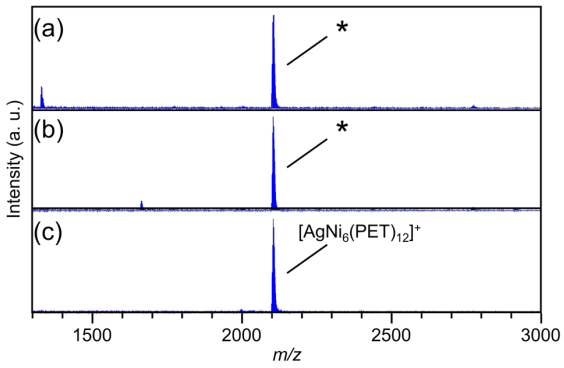

Fig. S14 Positive-ion MALDI-MS spectra of (a) $Ni_4(PET)_8$, (b) $Ni_5(PET)_{10}$ and (c) $Ni_6(PET)_{12}$ after the addition of Ag ions. The peaks with "*" was assigned as $[AgNi_6(PET)_{12}]^+$. These spectra demonstrate that no Ag ion can be included into $Ni_4(PET)_8$ and $Ni_5(PET)_{10}$.

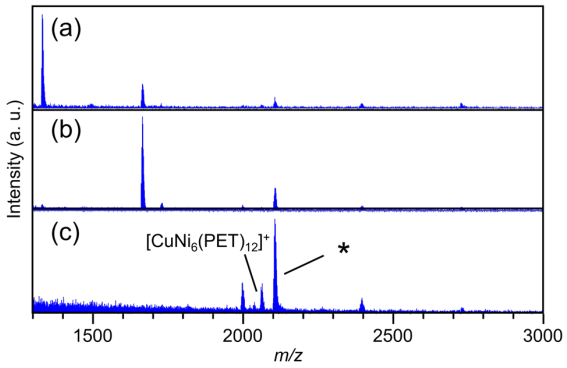

Fig. S15 Positive-ion MALDI-MS spectra of (a) $Ni_4(PET)_8$, (b) $Ni_5(PET)_{10}$ and (c) $Ni_6(PET)_{12}$ after addition of Cu ions. The peaks with "*" assigned as $[AgNi_6(PET)_{12}]^+$ due to the contamination of Ag ion on the measurement plate for MALDI. These spectra demonstrate that no Cu ion can be included into $Ni_4(PET)_8$ and $Ni_5(PET)_{10}$.

6. Reference

[1] H. Asakura, S. Yamazoe, T. Misumi, A. Fujita, T. Tsukuda and T. Tanaka, *Radiat. Phys. Chem.*, 2020, **175**, 108270.

[2] M. J. Frisch, G. W. Trucks, H. B. Schlegel, G. E. Scuseria, M. A. Robb, J. R. Cheeseman, G. Scalmani, V. Barone, G. A. Petersson, H. Nakatsuji, X. Li, M. Caricato, A. V. Marenich, J. Bloino, B. G. Janesko, R. Gomperts, B. Mennucci, H. P. Hratchian, J. V. Ortiz, A. F. Izmaylov, J. L. Sonnenberg, D. Williams-Young, F. Ding, F. Lipparini, F. Egidi, J. Goings, B. Peng, A. Petrone, T. Henderson, D. Ranasinghe, V. G. Zakrzewski, J. Gao, N. Rega, G. Zheng, W. Liang, M. Hada, M. Ehara, K. Toyota, R. Fukuda, J. Hasegawa, M. Ishida, T. Nakajima, Y. Honda, O. Kitao, H. Nakai, T. Vreven, K. Throssell, J. A. Montgomery, Jr., J. E. Peralta, F. Ogliaro, M. J. Bearpark, J. J. Heyd, E. N. Brothers, K. N. Kudin, V. N. Staroverov, T. A. Keith, R. Kobayashi, J. Normand, K. Raghavachari, A. P. Rendell, J. C. Burant, S. S. Iyengar, J. Tomasi, M. Cossi, J. M. Millam, M. Klene, C. Adamo, R. Cammi, J. W. Ochterski, R. L. Martin, K. Morokuma, O. Farkas, J. B. Foresman, and D. J. Fox, GAUSSIAN 16 (Revision A.03), Gaussian, Inc., Wallingford, CT, 2016.

[3] H. G. M. Edwards, A. F. Johnson and I. R. Lewis, *Spectrochim. Acta, Part A*, 1993, **49**, 707–714.

[4] L. V. Nair, S. Hossain, S. Wakayama, S. Takagi, M. Yoshioka, J. Maekawa, A. Harasawa, B. Kumar, Y. Niihori, W. Kurashige and Y. Negishi, *J. Phys. Chem. C*, 2017, **121**, 11002–11009.

[5] J. Ji, G. Wang, T. Wang, X. You and X. Xu, *Nanoscale*, 2014, **6**, 9185–9191.

[6] A. M. S. Pembere, C. Cui, R. Anumula, H. Wu, P. An, T. Liang and Z. Luo, *Phys. Chem. Chem. Phys.*, 2019, **21**, 17933–17938.

[7] Q. Li, D. Wang, C. Han, X. Ma, Q. Lu, Z. Xing and X. Yang, *J. Mater. Chem. A*, 2018, **6**, 8233–8237.